ACS SENSORS

pubs.acs.org/acssensors

Article

Ultrasensitive Upconversion Nanoparticle Immunoassay for Human Serum Cardiac Troponin I Detection Achieved with Resonant Waveguide Grating

Yen-Ta Tseng, Yu-Chung Chiu, Van-Dai Pham, Wen-Hsuan Wu, Thanh Thu Le-Vu, Chih-Hsien Wang, Shiao-Wei Kuo, Michael W.Y. Chan, Chun-Hung Lin, Szu-Chin Li, Yi-Da Li, Hung-Chih Kan, Jiunn-Yuan Lin, Lai-Kwan Chau,* and Chia-Chen Hsu*

Cite This: *ACS Sens.* 2024, 9, 455−463

Read Online

ACCESS | Metrics & More | Article Recommendations | Supporting Information

ABSTRACT: Selective detection of biomarkers at low concentrations in blood is crucial for the clinical diagnosis of many diseases but remains challenging. In this work, we aimed to develop an ultrasensitive immunoassay that can detect biomarkers in serum with an attomolar limit of detection (LOD). We proposed a sandwich-type heterogeneous immunosensor in a 3 × 3 well array format by integrating a resonant waveguide grating (RWG) substrate with upconversion nanoparticles (UCNPs). UCNPs were used to label a target biomarker captured by capture antibody molecules immobilized on the surface of the RWG substrate, and the RWG substrate was used to enhance the upconversion luminescence (UCL) of UCNPs through excitation resonance. The LOD of the immunosensor was greatly reduced due to the increased UCL of UCNPs and the reduction of nonspecific adsorption of detection antibody-conjugated UCNPs on the RWG substrate surface by coating the RWG substrate surface with a carboxymethyl dextran layer. The immunosensor exhibited an extremely low LOD [0.24 fg/mL (9.1 aM)] and wide detection range (1 fg/mL to 100 pg/mL) in the detection of cardiac troponin I (cTnI). The cTnI concentrations in human serum samples collected at different times during cyclophosphamide, epirubicin, and 5-fluorouracil (CEF) chemotherapy in a breast cancer patient were measured by an immunosensor, and the results showed that the CEF chemotherapy did cause cardiotoxicity in the patient. Having a higher number of wells in such an array-based biosensor, the sensor can be developed as a high-throughput diagnostic tool for clinically important biomarkers.

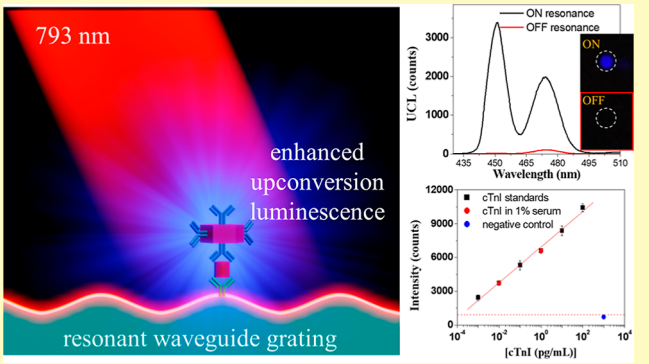

KEYWORDS: *resonant waveguide grating, excitation resonance, guided mode resonance, upconversion nanoparticle, upconversion luminescence, cardiac troponin I, sandwich-type heterogeneous immunoassay*

Lanthanide-ion doped upconversion nanoparticles (UCNPs) are attractive because they can convert near-infrared (NIR) excitation light to ultraviolet (UV), visible (Vis), or NIR emission through a cascaded multiphoton absorption process. UCNPs typically consist of a crystalline host, such as sodium yttrium tetrafluoride ($NaYF_4$), codoped with trivalent lanthanide ion sensitizers (ytterbium, Yb^{3+}, and neodymium, Nd^{3+}) and activators (erbium, Er^{3+}, thulium, Tm^{3+}, and holmium, Ho^{3+}). UCNPs have excellent photophysical properties, such as narrow emission lines, high photostability, no photobleaching, no autofluorescence, and low background signal.[1−6]

The use of UCNP fluorescent probes in bioassays can significantly reduce the limit of detection (LOD) to levels unattainable by conventional assays since UCNPs are excited by NIR light and assay biochemistry does not generate background luminescence.[7] Therefore, they are more suitable as fluorescent probes in biosensing applications than conventionally used organic dyes and quantum dots.[3−6,8−11] In addition, the UCL properties of UCNPs are inert to changes in buffer composition, sample matrix, and other environmental conditions.[7] UCNP-based bioassay research is becoming a flourishing field and various types of UCNP-based bioassays have emerged over the past two decades.[4−8,10−16] Sandwich-type heterogeneous biosensors are frequently developed because the use of a matched pair of antibodies provides the highest level of sensitivity and specificity.[7,17−22] Many studies

Received: October 23, 2023
Revised: December 15, 2023
Accepted: January 8, 2024
Published: January 18, 2024

have aimed to develop sandwich-type heterogeneous UCNP-based biosensors suitable for clinical and hospital diagnostic tools.[17−23]

Chemotherapy-induced-cardiotoxicity is a leading cause of death in cancer patients.[24,25] Cardiac troponin I (cTnI) is a contractile protein that is released into the circulation after a myocardial cell injury. Since cTnI is absent in skeletal muscle, it is considered as a sensitive and specific biomarker for myocardial infarction, including cardiotoxicity.[26−28] The level of cTnI is around 1 pg/mL for healthy people.[29] Due to the low concentration of cTnI in blood, an ultrasensitive assay is required to accurately quantify cTnI. However, the LODs of most sandwich-type heterogeneous UCNP-based biosensors are still in pg/mL to tens of ng/mL range,[17−21,23] which hinders their application in diagnosis of myocardial infarction and cardiotoxicity. Hence, there is a need to further improve the LOD of sandwich-type heterogeneous UCNP-based biosensors. Efforts have been made to reduce the assay LOD to below pg/mL by using various assays such as electrochemical assay,[30] electrochemiluminescence assay,[31] fluorescent immunoassays,[32,33] surface plasmon resonance assay,[34] optical microfiber-based label-free assay,[35] and UCNP-based immunoassays,[22,36] and single molecule array (Simoa) assay.[37,38] Among these assays, Simoa is being considered as a benchmark technology for high sensitivity detection and has been commercialized and used in clinical research in hospitals.[37,38] However, it requires a sophisticated instrument, expensive reagents, and tedious procedures for enzymatic amplification of signal and digital partitioning of test samples; thereby, a simpler and more direct method with equivalent or higher sensitivity is desirable.

All-dielectric resonant waveguide grating (RWG) is a nanograting waveguide structure that can exhibit sharp guided mode resonance (GMR).[39] RWG structures are frequently employed to facilitate light−mater interactions to generate strong emission from quantum dots,[40,41] fluorescent dyes,[42] UCNPs,[43] and nonlinear optical materials.[44,45] Recently, we showed that upconversion luminescence (UCL) of UCNPs placed on the surface of RWG can be enhanced more than 10^4 times due to the GMR-enhanced UCL of UCNPs.[46,47] Recently, the synergistic coupling of plasmonic and RWG photonic modes was employed to enhance the emission of fluorophore-coated-plasmonic nanoparticles.[48] The approach effectively reduced the LOD of a sandwich type immunoassay to the 10 fg/mL level.[48] These findings inspired us to use RWG structures to improve the detection sensitivity of the sandwich-type heterogeneous UCNP-based biosensor.

In this work, we present a novel sandwich-type heterogeneous RWG-UCNP immunosensor reported for the first time that can detect biomarkers in serum with attomolar LOD. The immunosensor consists of a RWG substrate and an UCNP fluorescent probe. The RWG substrate is used to amplify the UCL of the UCNPs. Figure 1a illustrates the concept of the enhancement of UCL of the UCNP fluorescent probes, in which strong excitation light is formed on top of the RWG substrate when the wavelength and the incident angle of the excitation light match the RWG resonance coupling condition. As a result, the UCL of UCNPs can be greatly enhanced, thereby significantly improving the detection sensitivity of bioassays. Figure 1b depicts the design of the 3 × 3 RWG-UCNP immunosensor. In each well, capture antibody molecules (anticardiac troponin I) are immobilized on the RWG surface to capture cTnI and UCNP-conjugated

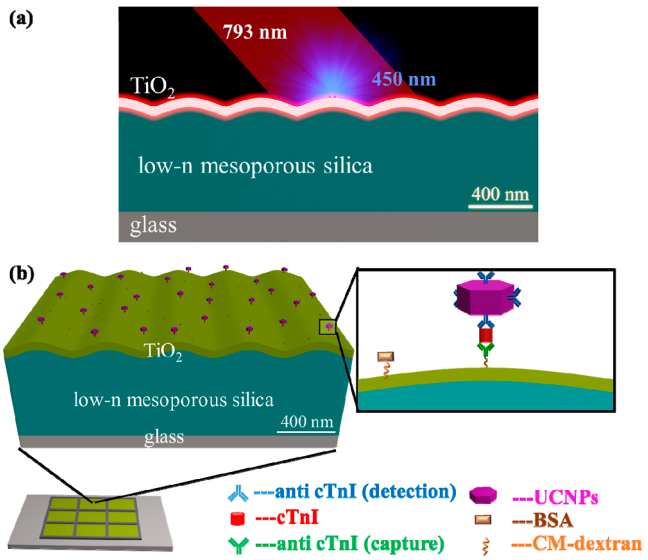

Figure 1. (a) Illustration of the concept of the enhancement of the UCL of the UCNP fluorescent probes. (b) Design of the 3 × 3 RWG-UCNP immunosensor for the detection of cTnI.

detection antibody forming a sandwich structure. Using the RWG-UCNP immunosensor to detect cTnI, the LOD can reach 0.24 fg/mL, which is approximately 54 times lower than the benchmark cTnI detection result obtained by Simoa.[38] Compared with Simoa, our approach has the following advantages: it is cost-effective and does not require enzymatic amplification of the signal and digital partitioning of test samples.

EXPERIMENTAL SECTION

Materials and Reagents. Details about the chemicals and materials used in this work are described in Supporting Information S1. Monoclonal mouse antihuman cardiac troponin I antibody 560 cm^3 (detection antibody Ab^D, IgG1, amino acid range, a.a.r., 83−93) and 19C7 cm^3 (capture antibody Ab^C, IgG2b, a.a.r. 41−49) were purchased from HyTest (catalog: 4T21/4T21 cm^3, Finland). Standard full-length (a.a.r. 1−210) recombinant human cardiac troponin I protein (cTnI, ab283299, 26.4 kDa) was obtained from Abcam (UK). Human serum H4522 was from Merck Sigma-Aldrich.

Synthesis and Characterization of Detection Antibody-Conjugated UCNPs. In this work, $NaYF_4$:Yb^{3+}(20%),Tm^{3+}(2%)@$NaYF_4$:Yb^{3+},Nd^{3+}(40%)@$NaYF_4$ core−double-shell UCNPs were selected for their strong UCL emission.[47] Oleic acid (OA)-functionalized core-double-shell $NaYF_4$:Yb^{3+},Tm^{3+}@$NaYF_4$:Yb^{3+},Nd^{3+}@$NaYF_4$ UCNPs (OA-UCNPs) were synthesized according to the recipe reported in our previous study[47] and the details of the synthesis and characterization are presented in Supporting Information S2.1 and S2.2.

To disperse UCNPs into water, the OA on UCNPs were replaced with poly(acrylic acid) (PAA) to form PAA-terminated core-double-shell UCNPs (PAA-UCNPs). Details of PAA-UCNP synthesis are described in Supporting Information S2.3.

To prepare detection antibody-conjugated UCNPs (UCNP@Ab^D) as shown in Figure 1b, the carboxylic acid of PAA-UCNPs was used to conjugate to one amino group of the detection antibody (Ab^D) via carbodiimide coupling (see Figure S1a). Details of the UCNP@Ab^D synthesis are described in Supporting Information S2.4.

Simulation, Fabrication, Characterization, and Surface Modification of RWG Substrate. *Simulation of RWG Substrate.* Rigorous coupled wave approximation (RCWA) simulation (RSoft CAD) was performed to assist in the design of the RWG substrate. The aim of the simulation is that a strong local field enhancement occurs on the RWG substrate surface when the excitation light

https://doi.org/10.1021/acssensors.3c02240
ACS Sens. 2024, 9, 455−463

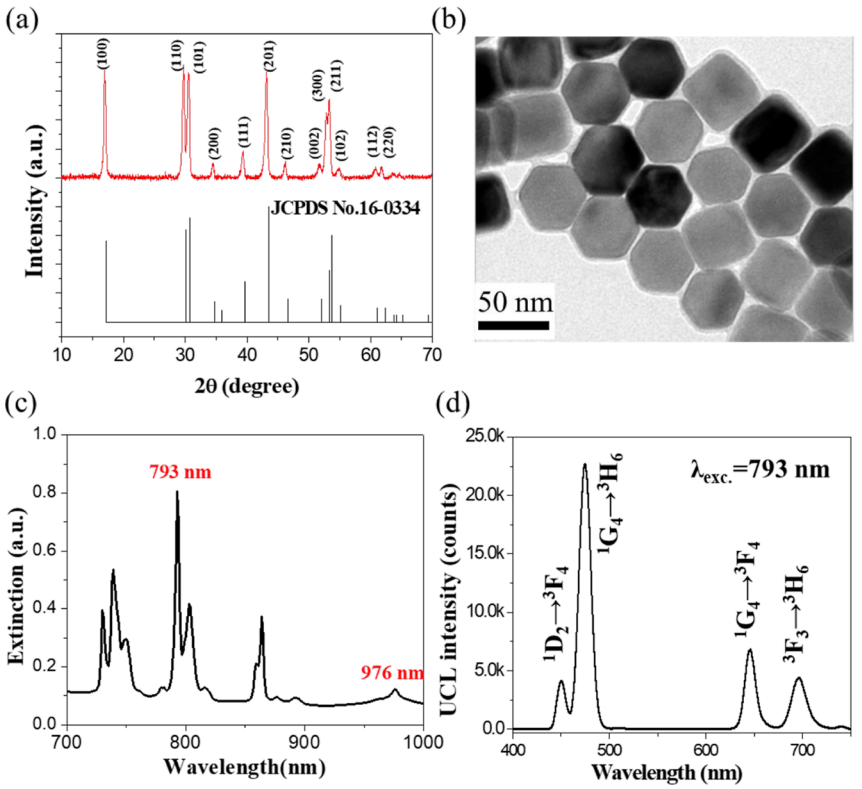

Figure 2. Characterization results of core−double-shell OA-UCNPs: (a) XRD pattern, (b) TEM image, (c) extinction spectrum, and (d) UCL spectrum.

matches the GMR resonance conditions. Table S1 and Figure S2 show the structural parameters and the refractive index distribution contour map of the RWG substrate used for the RCWA simulation, respectively. In the simulation, the polarization of the incident light is in the transverse electric (TE) mode.

Preparation of RWG Substrate. Figure S3 shows the preparation process of the RWG substrate. Details are described in Supporting Information S2.5.

Characterization of RWG Substrate. Atomic force microscopy (AFM, XE70, Park systems) was used to characterize the morphology of the grating fabricated on the low-refractive-index (low-n) mesoporous silica film. The TE mode transmission spectra of the RWG substrate covered with water and a coverslip were measured at different incident angles to search for the GMR at a wavelength of 793 nm. Spectral measurements were performed with a spectrometer (Andor Shamrock SR 500i) equipped with a CCD detector (DV401A-BV, Andor).

Preparation of Capture Antibody-Functionalized 3 × 3 Well Array Chip. The RWG substrate was divided into a 3 × 3 well array to facilitate the detection of multiple samples (including blanks) using a single 3 × 3 well array chip. Figure S1b,c shows the preparation process for the 3 × 3 well array chip. Details of the procedure are described in Supporting Information S2.6.

Preparation of Samples. First, the cTnI standard was serially diluted with PBS to obtain seven different concentrations of cTnI standard solutions ranging from 10^{-3} to 10^{2} pg/mL. Next, these cTnI standard solutions were individually mixed with a UCNP@Ab^{D} solution to form the UCNP@Ab^{D}−cTnI complex (see Figure S1a). Then, these standard solutions and two blank PBS solutions (40 μL each) were separately loaded into each well to form the sandwich nanocomplex UCNP@Ab^{D}−cTnI−Ab^{C} on the RWG substrate, followed by UCL measurement to construct a calibration curve (see Figure S1c).

To evaluate the selectivity of this system, 50 μL of human serum was first diluted 100-fold with a mixture of PBS and a UCNP@Ab^{D} solution. Next, 50 μL of cTnI at two different concentrations (1 pg/mL and 100 pg/mL) were separately added to the resulting solution to get two serum solution samples at final cTnI concentrations of 0.01 and 1.00 pg/mL. To prepare the negative control sample, a similar preparation procedure as for the cTnI standard solutions was used except that cTnI was replaced by the biomarker of heart failure: The N-terminal prohormone brain natriuretic peptide (NT-proBNP), at a concentration of 1 ng/mL. To prepare the cTnI-spiked serum sample, a 50 μL cTnI solution (100 pg/mL) was spiked into 50 μL human serum (H4522, Sigma), and diluted with PBS buffer (pH 7.2) to 5 mL so that the final cTnI concentration was 1 pg/mL.

Following a similar procedure to the spiked serum samples, the patient serum samples were diluted with PBS without the addition of cTnI. To evaluate the cardiotoxicity of epirubicin for chemotherapy treatment, four serum samples were collected from a 75 year-old woman with breast cancer who received chemotherapy with cyclophosphamide, epirubicin, and 5-fluorouracil (CEF) every 3 weeks up to 18 weeks. These serum samples were collected before treatment (0m), 3 months (3m), 6 months (6m), and 12 months (12m) after treatment. In addition, four serum samples were collected from the other patients. The cTnI concentration of the samples were determined by using both the proposed method and the standard clinical laboratory chemiluminescent microparticle immunoassay (CMIA) method (Abbott ARCHITECT STAT Troponin I). All human plasma samples were collected according to a protocol (IRB A10603002) approved by the Institutional Review Board of the Dalin Tzu Chi Hospital, Taiwan. The method of obtaining human serum is the same as that of routine operation in hospital.

UCL Measurements of Samples. Figure S4 shows the experimental setup for UCL measurements of samples in a 3 × 3 well array. Samples were excited by using a CW laser diode (Lumics, LU 0793M250) at 793 nm. The output laser beam was collimated by using a fiber collimator (CFC8X-B, Thorlabs) to obtain a beam diameter of 1.4 mm. Using a half-wave plate and polarizer combination fixed the excitation power and the polarization of the excitation laser at 180 mW and TE polarization, respectively. Then, the collimated laser beam was illuminated on the sample at a GMR

https://doi.org/10.1021/acssensors.3c02240
ACS Sens. 2024, 9, 455−463

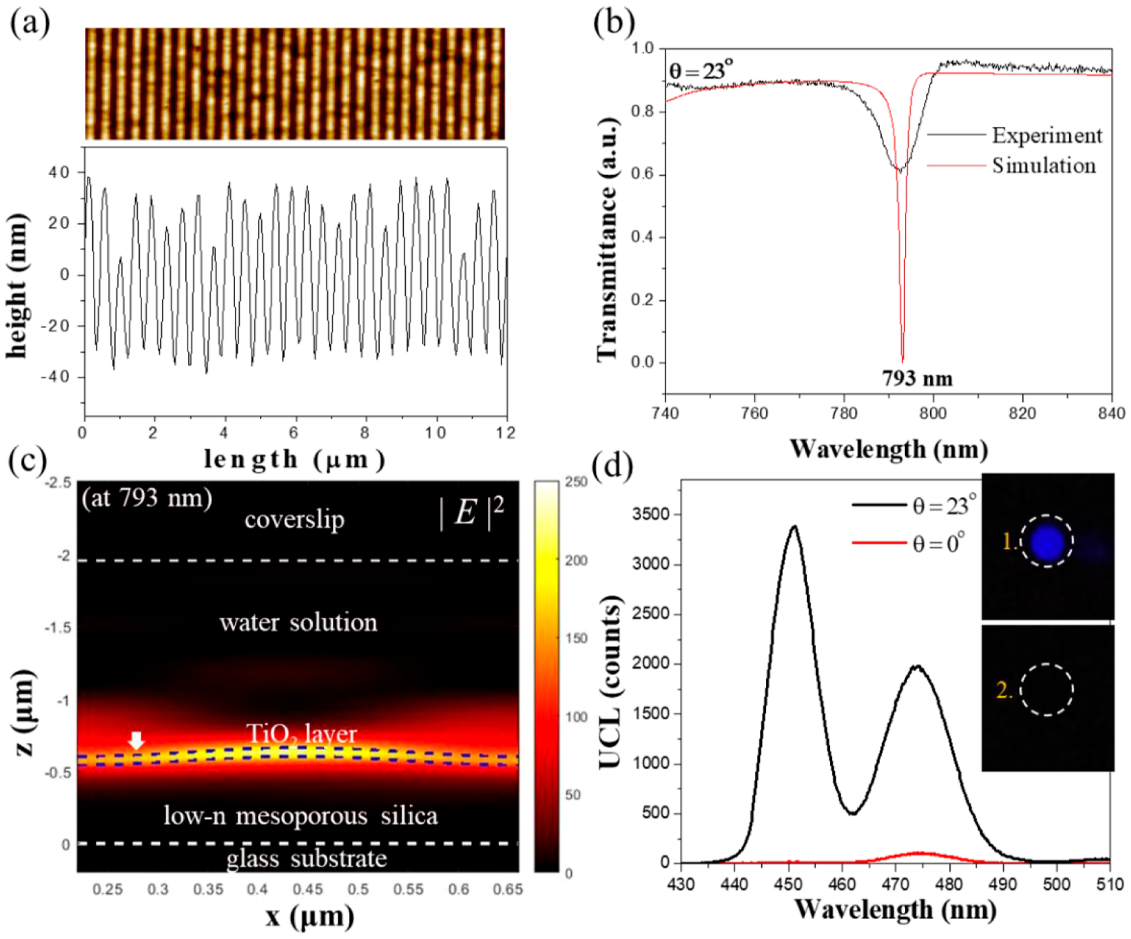

Figure 3. (a) Top panel: AFM image of the RWG substrate. Bottom panel: the height line profile extracted from the AFM image. (b) Simulated and measured TE mode transmission spectra of the RWG substrate covered with water solution at an incident angle of $\theta = 23°$. (c) Cross-sectional view of the simulated electric field intensity distribution of TE polarized incident light in an RWG substrate covered with water solution for $\theta = 23°$ and excitation wavelength $\lambda = 793$ nm. (d) UCL spectra from an RWG-UCNP immunosensor with [cTnI] of 10 fg/mL collected at $\theta = 23°$ and $\theta = 0°$. Inset: UCL images of the sample obtained under resonant excitation (top panel) and off-resonant excitation (bottom panel).

angle (23°). Using a pair of lenses, the UCL of the sample was collected at a detection angle of 70° and focused onto an optical fiber coupled to the spectrometer (Andor Shamrock SR 500i). In front of the fiber coupler of the spectrometer, a short pass filter (FES0550, Thorlabs) and an IR filter (short-pass, OD4-750 nm, Edmund Optics) were used to block the excitation laser light. The same experimental conditions were used for the UCL spectra measurement of all samples, namely, excitation power, excitation and detection angles, set temperature, acquisition time, CCD gain, etc.

RESULTS AND DISCUSSION

Characterization of Core−double-shell UCNPs. In the inner shell ($NaYF_4$:Yb^{3+},Nd^{3+}) of the UCNPs, Nd^{3+} ions act as sensitizers to absorb NIR excitation light at 793 nm, and then, the absorption energy is transferred to nearby Yb^{3+} ions through the Nd^{3+} (inner shell) → Yb^{3+} (inner shell) energy transfer process. Then, the energy possessed by Yb^{3+} ions is transferred to the Tm^{3+} activators in the core through the Yb^{3+} (inner shell) → Yb^{3+} (core) → Tm^{3+} (core) energy transfer process. The outer inert shell $NaYF_4$ plays a role in reducing surface quenching of excited ions and improving UCL efficiency.

Figure 2a shows the XRD pattern of the core−double-shell OA-UCNPs, which is identical to that of the JCPDS no. 16-0334, indicating that the OA-UCNPs are with a high-purity $NaYF_4$ β-phase crystal structure. Figure 2b displays the TEM image of the OA-UCNPs, showing an extremely uniform particle size distribution with an average diameter of 43.0 ± 2.7 nm (Figure S5). Figure 2c shows the extinction spectrum of the core−double-shell OA-UCNPs in cyclohexene, showing an absorption peak at 793 nm higher than that at 976 nm. This reveals that Nd^{3+} ions have a larger absorption cross-section than Yb^{3+}ions. Figure 2d displays the UCL spectrum of the OA-UCNPs in cyclohexene under 793 nm laser excitation, and the emission peaks appear at 450, 475, 645, and 695 nm, corresponding to the energy transitions of the Tm^{3+} ion shown in Figure 2d. From these characterization results, we confirm that the UCNPs have suitable properties for use as fluorescent probes and can be excited by a low-power CW laser at 793 nm to produce high intensity UCL.

Simulation and Characterization of RWG Substrate. Figure S6 shows an SEM image of the RWG substrate. From the AFM image of the RWG substrate shown in Figure 3a, the average period and average depth of the RWG substrate were determined to be 441.2 and 62.6 nm, respectively. Figure 3b illustrates the simulated and measured TE mode transmission spectra of the RWG substrate covered with water solution at an incident angle of $\theta = 23°$. Both spectra have a transmission dip at 793 nm, confirming the occurrence of GMR at a wavelength of 793 nm. As shown in Figure 3b, the experimentally

https://doi.org/10.1021/acssensors.3c02240
ACS Sens. 2024, 9, 455−463

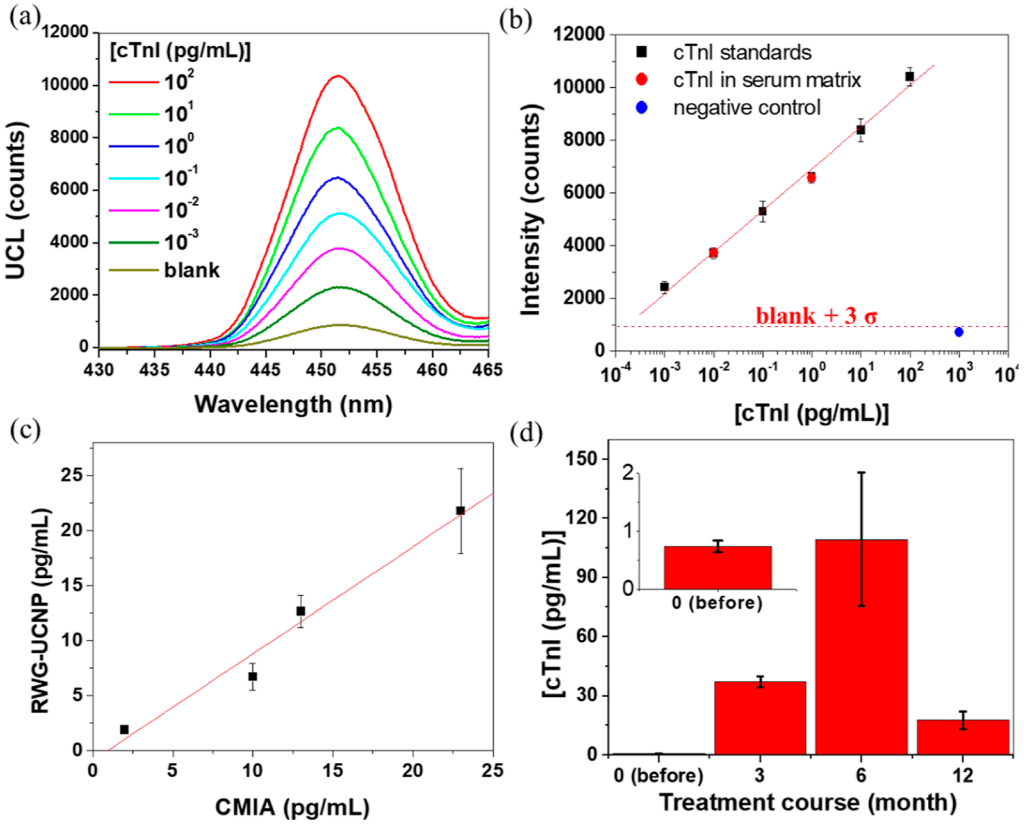

Figure 4. (a) UCL spectra of standard solutions of [cTnI] from 10^{-3} to 10^{2} pg/mL in 3 × 3 well array chips. (b) Average UCL peak intensity at 450 nm vs [cTnI] in PBS (black squares) obtained from three different chips (N = 3); calibration curve (solid red line), serum solution samples containing 0.01 and 1.00 pg/mL of cTnI (red circles), and negative control sample (blue circle). (c) A plot displaying the correlation between the results from RWG-UCNP and CMIA methods for the detection of cTnI in serum samples. (d) Follow-up analysis of [cTnI] in a patient receiving CEF chemotherapy. Note all the data shown in (b–d) are the averages of three experimental results.

measured transmission dip is not as narrow and deep as the simulation. We speculate that the uneven modulation depth of the grating structure (as shown in Figure 3a) and the imperfectly collimated white light used in the transmission spectrum measurement may be the reasons for the broadening and shallowing of the experimentally measured transmission dip. Figure 3c shows the simulation of the electric field intensity ($|E|^2$) distribution of TE polarized incident light in the RWG substrate under the GMR excitation condition. Due to the reverse symmetry of the waveguide structure design, a strong local field is formed in the TiO_2 layer and extends to the water solution region. This local electric field enhancement results in a greatly enhanced UCL intensity of UCNPs in RWG-UCNP sandwich immunosensors. Figure 3d compares the UCL spectra of the RWG-UCNP immunosensor with a cTnI concentration ([cTnI]) of 10 fg/mL, acquired at θ = 23° (resonant excitation) and θ = 0° (nonresonant excitation). The result confirmed that the resonant excitation greatly enhanced the UCL intensity of UCNPs with an enhancement factor of about 200 times. Top and bottom inset panels show UCL images of the sample acquired at θ = 23° and θ = 0°, respectively. From these characterization results, we confirm that the RWG substrate has been successfully fabricated and has GMR at the wavelength of 793 nm. Most importantly, we confirm that the RWG substrate can greatly enhance the UCL of the UCNP fluorescent probes in the RWG-UCNP immunosensor.

Detection of cTnI. Figure 4a shows the UCL spectra of samples in a 3 × 3 well array chip as a function of cTnI concentration in PBS obtained under resonant excitation (θ = 23°). As shown, the UCL intensity of the samples increased with an increasing cTnI concentration. The black square points in Figure 4b are the average of the UCL peak intensity of the 450 nm band obtained from three different chips. The calibration curve (red solid line) of the RWG-UCNP immunosensor was obtained by linear regression of all data points to the linear equation (y = 1580x + 6925, R^2 = 0.99). The coefficient of variation (CV) for all data points is less than 10%, indicating that the method is reproducible even across different chips and in a 3 × 3 well array format. This array format allows the detection of multiple samples (including blanks) using a single well array chip and greatly increases the throughput of analysis.

In this study, a carboxymethyl dextran (CMD) layer was coated on the RWG substrate surface to minimize the background nonspecific adsorption of UCNP@Ab^D onto the sensor surface. Dextran has been shown to reduce nonspecific adsorption of proteins and protein-nanoparticle conjugates onto various sensor surfaces,[49−51] while the carboxyl groups in CMD provide the binding sites for Ab^C conjugation. To eliminate false positive signals due to nonspecific adsorption of UCNP@Ab^D onto the RWG substrate surface, we define a threshold value B + 3σ, where B and σ are the average and the standard deviation of the blank, respectively. This threshold is represented by the horizontal dashed line in Figure 4b and was

https://doi.org/10.1021/acssensors.3c02240
ACS Sens. 2024, 9, 455−463

Table 1. Comparison of UCNP Bioassays for cTnI Detection

methodology	UCNP	detection range (pg/mL)	LOD (pg/mL)	references
Fl (Eu^{3+})-LFA[a]	$GdVO_4$:30%Eu	0−20,000	17	19
UCNP-FLIA[b]	UCNP	30−10,000	30	20
digital ULISA[d]	$NaYF_4$:Yb^{3+},Er^{3+}	0−1,000,000	10	21
UCNP (Er^{3+})	$NaYF_4$:17%Yb^{3+},3%Er^{3+}	0.05−50,000	0.13	22
ULISA[c]	$NaYF_4$:Yb^{3+},Tm^{3+}@$NaYF_4$	10−10,000,000	130	23
RWG-UCNP	$NaYF_4$:Yb^{3+},Tm^{3+}@$NaYF_4$:Yb^{3+},Nd^{3+}@$NaYF_4$	0.001−1,00	0.00024	this work

[a]Fluorescence-based lateral flow assay. [b]Upconverting nanoparticle-lateral flow immunoassay. [c]Upconversion-linked immunoassay. [d]Single-molecule (digital) upconverting nanoparticle immunoassay.

also used to calculate the LOD by finding the intersection of the calibration curve and the horizontal dashed line. Thus, the LOD for cTnI detection in PBS was 0.24 fg/mL (9.1 aM) indicating that our method is capable of detecting as few as approximately 2.2×10^2 cTnI molecules (cTnI molecular weight = 26.4 kDa, well volume = 40 μL). In comparison with a benchmark cTnI assay based on single molecule array (Simoa) which exhibits a LOD of 13 fg/mL,[38] the LOD of our method is about 54 times lower. Compared with Simoa, our approach is cost-effective and does not require enzymatic amplification of the signal and digital partitioning of test samples.

To understand matrix effects and demonstrate the applicability of the proposed method to real samples, two human serum samples were diluted 100-fold with PBS with known cTnI concentrations (1 and 10^{-2} pg/mL) as testing samples. The UCL signals of these two testing samples (red circles) are comparable to those obtained in PBS buffer, with recoveries of 98.87% ([cTnI] = 10^{-2} pg/mL) and 94.83% ([cTnI] = 1 pg/mL). This indicates that the serum matrix did not interfere with cTnI detection at 100-fold dilution. To investigate the specificity of this method, 1 ng/mL NT-proBNP in a PBS buffer was chosen as a negative control sample. As shown, the UCL signal of the negative control sample (blue circle in Figure 4b) was negligible, suggesting that the RWG-UCNP immunosensor had high specificity for detecting cTnI.

To address the feasibility of applying this method to real samples, we first tested it with a cTnI-spiked serum sample (see Figure S7). The result shows a good recovery of 99%, indicating that the method is applicable to serum samples. To further investigate the quantitation accuracy of the method, four serum specimens from patients were validated with the clinically accepted CMIA method in a blinded manner. The results obtained from these two methods show a good correlation coefficient of 0.986 from the linear regression analysis, as shown in Figure 4c, indicating that the results are highly correlated. The regression line of the plot in Figure 4c has a slope of 0.972 and an intercept of 0.905, suggesting that proportional bias and constant bias, respectively, between these two methods are small. After validation of our method, we measured cTnI concentrations in human serum specimens collected from a breast cancer patient at different times during CEF chemotherapy treatment. Figure 4d shows that pretreatment (0 month) [cTnI] was below 1.0 pg/mL. However, [cTnI] increased to 37.2 and 109.5 pg/mL after 3 and 6 months of treatment, respectively. Finally, [cTnI] dropped to 17.7 pg/mL after 12 months of treatment because the treatment course lasted only for 4.5 months. The results showed that CEF chemotherapy did cause cardiotoxicity in the patient, as reported in previous study.[52]

Table 1 summarizes a comparison of the RWG-UCNP immunosensor with other UCNP-based bioassays. The detection range of our method is comparable to those of previously reported UCNP-based bioassays, while our LOD is several orders of magnitude lower than reported values, which is attributed to the GMR-enhanced UCL of UCNPs provided by the RWG substrate.

CONCLUSIONS

In this study, we utilized an RWG substrate to enhance the UCL of the UCNP fluorescent probes in the immunoassay and achieved cTnI detection LOD at subfg/mL level with a detection range of 6 orders of magnitude (1 fg/mL to 100 pg/L). We showed that the proposed UCNP-based immunoassay was highly specific for the detection of cTnI with negligible matrix effects on the serum matrix. In addition, the RWG substrate can easily be constructed to be an n x n well array, enabling detection of multiple samples using a single well array chip with a high throughput. cTnI concentrations were measured using an immunoassay in human serum samples collected from breast cancer patients at different times during CEF chemotherapy. Measurements showed that the cTnI concentration increased during CEF chemotherapy but returned to normal levels after CEF chemotherapy, confirming that CEF chemotherapy did cause cardiotoxicity in the patient. Overall, the proposed assay shows excellent performance in detecting low-concentration of biomarkers in serum and is expected to become an important diagnostic tool in hospitals and clinics.

ASSOCIATED CONTENT

Supporting Information

The Supporting Information is available free of charge at https://pubs.acs.org/doi/10.1021/acssensors.3c02240.

Reagents and materials, synthesis of OA-capped core−double-shell UCNPs, characterization of OA-UCNPs, surface-modification of OA-UCNPs by PAA, conjugation of detection antibody to PAA-UCNPs, preparation of the RWG substrate, preparation of capture antibody-functionalized 3 × 3 well array chip, structural parameters of the designed RWG substrate in the RCWA simulation, contour map of refractive index profile of the RWG substrate, experiment setup for UCL measurement of the RWG-UCNP sandwich immunoassay, size distribution of OA-UCNPs and SEM image of the RWG substrate, and testing on the cTnI-spiked human serum sample (PDF)

https://doi.org/10.1021/acssensors.3c02240
ACS Sens. 2024, 9, 455−463

AUTHOR INFORMATION

Corresponding Authors

Chia-Chen Hsu − *Department of Physics, National Chung Cheng University, Chia-Yi 621, Taiwan; Center for Nano Bio-Detection, National Chung Cheng University, Chia-Yi 621, Taiwan;* orcid.org/0000-0002-3014-8829; Email: phycch@ccu.edu.tw

Lai-Kwan Chau − *Department of Chemistry and Biochemistry and Center for Nano Bio-Detection, National Chung Cheng University, Chia-Yi 621, Taiwan;* orcid.org/0000-0002-1659-6465; Email: chelkc@ccu.edu.tw

Authors

Yen-Ta Tseng − *Department of Physics, National Chung Cheng University, Chia-Yi 621, Taiwan; Department of Chemistry and Biochemistry, National Chung Cheng University, Chia-Yi 621, Taiwan*

Yu-Chung Chiu − *Department of Physics, National Chung Cheng University, Chia-Yi 621, Taiwan*

Van-Dai Pham − *Department of Physics, National Chung Cheng University, Chia-Yi 621, Taiwan*

Wen-Hsuan Wu − *Department of Physics, National Chung Cheng University, Chia-Yi 621, Taiwan*

Thanh Thu Le-Vu − *Department of Physics, National Chung Cheng University, Chia-Yi 621, Taiwan*

Chih-Hsien Wang − *Department of Chemistry and Biochemistry, National Chung Cheng University, Chia-Yi 621, Taiwan*

Shiao-Wei Kuo − *Department of Materials and Optoelectronic Science, National Sun Yat Sen University, Kaohsiung 804, Taiwan;* orcid.org/0000-0002-4306-7171

Michael W.Y. Chan − *Center for Nano Bio-Detection and Department of Biomedical Sciences, National Chung Cheng University, Chia-Yi 621, Taiwan*

Chun-Hung Lin − *Department of Surgery, Dalin Tzu Chi Hospital, Buddhist Tzu Chi Medical Foundation, Chia-Yi 622, Taiwan*

Szu-Chin Li − *Department of Hematology and Oncology, Dalin Tzu Chi Hospital, Buddhist Tzu Chi Medical Foundation, Chia-Yi 622, Taiwan*

Yi-Da Li − *Department of Cardiology, Dalin Tzu Chi Hospital, Buddhist Tzu Chi Medical Foundation, Chia-Yi 622, Taiwan*

Hung-Chih Kan − *Department of Physics, National Chung Cheng University, Chia-Yi 621, Taiwan; Center for Nano Bio-Detection, National Chung Cheng University, Chia-Yi 621, Taiwan;* orcid.org/0000-0002-6203-9563

Jiunn-Yuan Lin − *Department of Physics, National Chung Cheng University, Chia-Yi 621, Taiwan*

Complete contact information is available at: https://pubs.acs.org/10.1021/acssensors.3c02240

Author Contributions

Yen-Ta Tseng: writing—original draft, methodology, and formal analysis. **Yu-Chung Chiu:** investigation and formal analysis. **Van-Dai Pham:** investigation and formal analysis. **Wen-Hsuan Wu:** investigation. **Thanh-Thu Le-Vu:** investigation. **Chih-Hsien Wang:** methodology. **Shiao-Wei Kuo:** resources. **Hung-Chih Kan:** methodology and writing—review and editing. **Jiunn-Yuan Lin:** methodology and writing—review and editing. **Michael W.Y. Chan:** resources, methodology, and writing—review and editing. **Chun-Hung Lin:** resources, **Szu-Chin Li:** resources, and **Yi-Da Li:** resources. **Lai-Kwan Chau:** conceptualization, methodology, and writing—review and editing. **Chia-Chen Hsu:** conceptualization, methodology, formal analysis, supervision, funding acquisition, and writing—review and editing.

Notes

The authors declare no competing financial interest.

ACKNOWLEDGMENTS

The authors acknowledge financial support from National Science and Technology Council (NSTC), Taiwan, under grant numbers MOST-110-2112-M-194-005, MOST 111-2112-M-194-007, MOST-106-2923-B-194-001-MY3, and MOST-111-2124-194-002. The authors gratefully acknowledge the Instruments Center of National Chung Cheng University (TEM/EM0000012200) for their support and assistance in this work. Dr. Yen-Ta Tseng acknowledges the support of postdoctoral fellowships from NSTC, Taiwan. Helpful discussion with Jhen-Jie Huang is acknowledged.

REFERENCES

(1) Wen, S.; Zhou, J.; Zheng, K.; Bednarkiewicz, A.; Liu, X.; Jin, D. Advances in Highly Doped Upconversion Nanoparticles. *Nat. Commun.* **2018**, *9* (1), 2415.

(2) Nguyen, V. N.; Lee, Y. H.; Le-Vu, T. T.; Lin, J. Y.; Kan, H. C.; Hsu, C. C. Impact of Excitation Intensity-Dependent Fluorescence Intensity Ratio of Upconversion Nanoparticles on Wide-Field Thermal Imaging. *ACS Appl. Nano Mater.* **2022**, *5* (10), 15172−15182.

(3) Liang, G.; Wang, H.; Shi, H.; Wang, H.; Zhu, M.; Jing, A.; Li, J.; Li, G. Recent Progress in the Development of Upconversion Nanomaterials in Bioimaging and Disease Treatment. *J. Nanobiotechnol.* **2020**, *18* (1), 154.

(4) Wang, J.; Sheng, T.; Zhu, X.; Li, Q.; Wu, Y.; Zhang, J.; Liu, J.; Zhang, Y. Spectral Engineering of Lanthanide-Doped Upconversion Nanoparticles and Their Biosensing Applications. *Mater. Chem. Front.* **2021**, *5* (4), 1743−1770.

(5) Wang, M.; Abbineni, G.; Clevenger, A.; Mao, C.; Xu, S. Upconversion Nanoparticles: Synthesis, Surface Modification and Biological Applications. *Nanomedicine* **2011**, *7* (6), 710−729.

(6) Chen, C.; Li, C.; Shi, Z. Current Advances in Lanthanide-Doped Upconversion Nanostructures for Detection and Bioapplication. *Adv. Sci.* **2016**, *3* (10), 1600029.

(7) Zhang, F. *Photon Upconversion Nanomaterials*; Nanostructure Science and Technology; Springer Berlin Heidelberg: Berlin, Heidelberg, 2015; Vol. 3.

(8) Vu, D. T.; Le, T. T. V.; Hsu, C. C.; Lai, N. D.; Hecquet, C.; Benisty, H. Positive Role of the Long Luminescence Lifetime of Upconversion Nanophosphors on Resonant Surfaces for Ultra-Compact Filter-Free Bio-Assays. *Biomed. Opt. Express* **2021**, *12* (1), 1.

(9) Vu, D. T.; Vu-Le, T. T.; Nguyen, V. N.; Le, Q. M.; Wang, C. R. C.; Chau, L. K.; Yang, T. S.; Chan, M. W. Y.; Lee, C. I.; Ting, C. C.; Lin, J. Y.; Kan, H. C.; Hsu, C. C. Gold Nanorods Conjugated Upconversion Nanoparticles Nanocomposites for Simultaneous Bioimaging, Local Temperature Sensing and Photothermal Therapy of OML-1 Oral Cancer Cells. *Int. J. Smart Nano Mater.* **2021**, *12* (1), 49−71.

(10) Mickert, M. J.; Farka, Z.; Kostiv, U.; Hlaváček, A.; Horák, D.; Skládal, P.; Gorris, H. H. Measurement of Sub-Femtomolar Concentrations of Prostate-Specific Antigen through Single-Molecule Counting with an Upconversion-Linked Immunosorbent Assay. *Anal. Chem.* **2019**, *91* (15), 9435−9441.

(11) Lin, G.; Jin, D. Responsive Sensors of Upconversion Nanoparticles. *ACS Sens.* **2021**, *6* (12), 4272−4282.

(12) DaCosta, M. V.; Doughan, S.; Han, Y.; Krull, U. J. Lanthanide Upconversion Nanoparticles and Applications in Bioassays and Bioimaging: A Review. *Anal. Chim. Acta* **2014**, *832*, 1−33.

(13) Hao, S.; Chen, G.; Yang, C. Sensing Using Rare-Earth-Doped Upconversion Nano-Particles. *Theranostics* **2013**, *3* (5), 331−345.
(14) Borse, S.; Rafique, R.; Murthy, Z. V. P.; Park, T. J.; Kailasa, S. K. Applications of Upconversion Nanoparticles in Analytical and Biomedical Sciences: A Review. *Analyst* **2022**, *147* (14), 3155−3179.
(15) Chen, G.; Qiu, H.; Prasad, P. N.; Chen, X. Upconversion Nanoparticles: Design, Nanochemistry, and Applications in Theranostics. *Chem. Rev.* **2014**, *114* (10), 5161−5214.
(16) Liu, Y.; Tu, D.; Zhu, H.; Ma, E.; Chen, X. Lanthanide-Doped Luminescent Nano-Bioprobes: From Fundamentals to Biodetection. *Nanoscale* **2013**, *5* (4), 1369−1384.
(17) Liu, Z.; Yang, B.; Chen, B.; He, M.; Hu, B. Upconversion Nanoparticle as Elemental Tag for the Determination of Alpha-Fetoprotein in Human Serum by Inductively Coupled Plasma Mass Spectrometry. *Analyst* **2017**, *142* (1), 197−205.
(18) He, W.; You, M.; Li, Z.; Cao, L.; Xu, F.; Li, F.; Li, A. Upconversion Nanoparticles-Based Lateral Flow Immunoassay for Point-of-Care Diagnosis of Periodontitis. *Sens. Actuators, B* **2021**, *334* (February), 129673.
(19) Chen, L.; Zhou, S.-Y.; Zhu, W.; Liu, S.-P.; Zhang, J.-X.; Zhuang, H.; Zhang, J. L.; Li, Y. S.; Gao, F. Highly Sensitive Lanthanide-Doped Nanoparticles-Based Point-of-Care Diagnosis of Human Cardiac Troponin I. *Int. J. Nanomed.* **2022**, *17*, 635−646.
(20) Bayoumy, S.; Martiskainen, I.; Heikkilä, T.; Rautanen, C.; Hedberg, P.; Hyytiä, H.; Wittfooth, S.; Pettersson, K. Sensitive and Quantitative Detection of Cardiac Troponin I with Upconverting Nanoparticle Lateral Flow Test with Minimized Interference. *Sci. Rep.* **2021**, *11* (1), 18698.
(21) Brandmeier, J. C.; Raiko, K.; Farka, Z.; Peltomaa, R.; Mickert, M. J.; Hlaváček, A.; Skládal, P.; Soukka, T.; Gorris, H. H. Effect of Particle Size and Surface Chemistry of Photon-Upconversion Nanoparticles on Analog and Digital Immunoassays for Cardiac Troponin. *Adv. Healthc. Mater.* **2021**, *10* (18), 2100506.
(22) Raiko, K.; Lyytikäinen, A.; Ekman, M.; Nokelainen, A.; Lahtinen, S.; Soukka, T. Supersensitive Photon Upconversion Based Immunoassay for Detection of Cardiac Troponin I in Human Plasma. *Clin. Chim. Acta* **2021**, *523* (October), 380−385.
(23) Shapoval, O.; Brandmeier, J. C.; Nahorniak, M.; Oleksa, V.; Makhneva, E.; Gorris, H. H.; Farka, Z.; Horák, D. PMVEMA-Coated Upconverting Nanoparticles for Upconversion-Linked Immunoassay of Cardiac Troponin. *Talanta* **2022**, *244* (March), 123400.
(24) Gasser, A.; Chen, Y. W.; Audebrand, A.; Daglayan, A.; Charavin, M.; Escoubet, B.; Karpov, P.; Tetko, I.; Chan, M. W. Y.; Cardinale, D.; Désaubry, L.; Nebigil, C. G. Prokineticin Receptor-1 Signaling Inhibits Dose- and Time-Dependent Anthracycline-Induced Cardiovascular Toxicity Via Myocardial and Vascular Protection. *JACC* **2019**, *1* (1), 84−102.
(25) Kumari, H.; Huang, W. H.; Chan, M. W. Y. Review on the Role of Epigenetic Modifications in Doxorubicin-Induced Cardiotoxicity. *Front. Cardiovasc. Med.* **2020**, *7* (May), 56.
(26) Kim, L. J.; Martinez, E. A.; Faraday, N.; Dorman, T.; Fleisher, L. A.; Perler, B. A.; Williams, G. M.; Chan, D.; Pronovost, P. J. Cardiac Troponin I Predicts Short-Term Mortality in Vascular Surgery Patients. *Circulation* **2002**, *106* (18), 2366−2371.
(27) Balmagambetova, S.; Tlegenova, Z.; Zholdin, B.; Kurmanalina, G.; Talipova, I.; Koyshybaev, A.; Nurmanova, D.; Sultanbekova, G.; Baspayeva, M.; Madinova, S.; Kubenova, K.; Urazova, A. Early Diagnosis of Chemotherapy-Linked Cardiotoxicity in Breast Cancer Patients Using Conventional Biomarker Panel: A Prospective Study Protocol. *Diagnostics* **2022**, *12* (11), 2714.
(28) Han, X.; Li, S.; Peng, Z.; Othman, A. M.; Leblanc, R. Recent Development of Cardiac Troponin I Detection. *ACS Sens.* **2016**, *1* (2), 106−114.
(29) Fathil, M. F. M.; Md Arshad, M. K.; Gopinath, S. C. B.; Hashim, U.; Adzhri, R.; Ayub, R. M.; Ruslinda, A. R.; Nuzaihan M.N, M.; Azman, A. H.; Zaki, M.; Tang, T. H. Diagnostics on Acute Myocardial Infarction: Cardiac Troponin Biomarkers. *Biosens. Bioelectron.* **2015**, *70*, 209−220.
(30) Lv, H.; Li, Y.; Zhang, X.; Li, X.; Xu, Z.; Chen, L.; Li, D.; Dong, Y. Thionin Functionalized Signal Amplification Label Derived Dual-Mode Electrochemical Immunoassay for Sensitive Detection of Cardiac Troponin I. *Biosens. Bioelectron.* **2019**, *133* (January), 72−78.
(31) Zhan, T.; Su, Y.; Lai, W.; Chen, Z.; Zhang, C. A Dry Chemistry-based Ultrasensitive Electrochemiluminescence Immunosensor for Sample to Answer detection of Cardiac Troponin I. *Biosens. Bioelectron.* **2022**, *214* (June), 114494.
(32) Kar, P.; Pandey, A.; Greer, J. J.; Shankar, K. Ultrahigh Sensitivity Assays for Human Cardiac Troponin I Using TiO_2 Nanotube Arrays. *Lab Chip* **2012**, *12* (4), 821.
(33) Tran, V. T.; Ju, H. Fluorescence Based on Surface Plasmon Coupled Emission for Ultrahigh Sensitivity Immunoassay of Cardiac Troponin I. *Biomedicines* **2021**, *9* (5), 448.
(34) Çimen, D.; Bereli, N.; Günaydın, S.; Denizli, A. Detection of Cardiac Troponin-I by Optic Biosensors with Immobilized Anti-Cardiac Troponin-I Monoclonal Antibody. *Talanta* **2020**, *219* (April), 121259.
(35) Zhou, W.; Li, K.; Wei, Y.; Hao, P.; Chi, M.; Liu, Y.; Wu, Y. Ultrasensitive Label-Free Optical Microfiber Coupler Biosensor for Detection of Cardiac Troponin I Based on Interference Turning Point Effect. *Biosens. Bioelectron.* **2018**, *106* (October 2017), 99−104.
(36) Lahtinen, S.; Lyytikäinen, A.; Sirkka, N.; Päkkilä, H.; Soukka, T. Improving the Sensitivity of Immunoassays by Reducing Non-Specific Binding of Poly(Acrylic Acid) Coated Upconverting Nanoparticles by Adding Free Poly(Acrylic Acid). *Microchim. Acta* **2018**, *185* (4), 220.
(37) Empana, J. P.; Lerner, I.; Perier, M. C.; Guibout, C.; Jabre, P.; Bailly, K.; Andrieu, M.; Climie, R.; van Sloten, T.; Vedie, B.; Geromin, D.; Marijon, E.; Thomas, F.; Danchin, N.; Boutouyrie, P.; Jouven, X. Ultrasensitive Troponin I and Incident Cardiovascular Disease. *Arterioscler., Thromb., Vasc. Biol.* **2022**, *42* (12), 1471−1481.
(38) Jarolim, P.; Patel, P. P.; Conrad, M. J.; Chang, L.; Melenovsky, V.; Wilson, D. H. Fully Automated Ultrasensitive Digital Immunoassay for Cardiac Troponin I Based on Single Molecule Array Technology. *Clin. Chem.* **2015**, *61* (10), 1283−1291.
(39) Wang, S. S.; Magnusson, R. Theory and Applications of Guided-Mode Resonance Filters. *Appl. Opt.* **1993**, *32* (14), 2606.
(40) Ganesh, N.; Zhang, W.; Mathias, P. C.; Chow, E.; Soares, J. A. N. T.; Malyarchuk, V.; Smith, A. D.; Cunningham, B. T. Enhanced Fluorescence Emission from Quantum Dots on a Photonic Crystal Surface. *Nat. Nanotechnol.* **2007**, *2* (8), 515−520.
(41) Xiong, Y.; Huang, Q.; Canady, T. D.; Barya, P.; Liu, S.; Arogundade, O. H.; Race, C. M.; Che, C.; Wang, X.; Zhou, L.; Wang, X.; Kohli, M.; Smith, A. M.; Cunningham, B. T. Photonic Crystal Enhanced Fluorescence Emission and Blinking Suppression for Single Quantum Dot Digital Resolution Biosensing. *Nat. Commun.* **2022**, *13* (1), 4647.
(42) Pokhriyal, A.; Lu, M.; Chaudhery, V.; Huang, C. S.; Schulz, S.; Cunningham, B. T. Photonic Crystal Enhanced Fluorescence Using a Quartz Substrate to Reduce Limits of Detection. In *CLEO:2011—Laser Applications to Photonic Applications*; OSA: Washington, D.C., 2011; p CThQ1.
(43) Lin, J. H.; Liou, H. Y.; Wang, C. D.; Tseng, C. Y.; Lee, C. T.; Ting, C. C.; Kan, H. C.; Hsu, C. C. Giant Enhancement of Upconversion Fluorescence of $NaYF_4$:Yb^{3+},Tm^{3+} Nanocrystals with Resonant Waveguide Grating Substrate. *ACS Photonics* **2015**, *2* (4), 530−536.
(44) Lin, J. H.; Tseng, C. Y.; Lee, C. T.; Kan, H. C.; Hsu, C. C. Guided-Mode Resonance Enhanced Excitation and Extraction of Two-Photon Photoluminescence in a Resonant Waveguide Grating. *Opt. Express* **2013**, *21* (20), 24318.
(45) Lin, J. H.; Tseng, C. Y.; Lee, C. T.; Young, J. F.; Kan, H. C.; Hsu, C. C. Strong Guided Mode Resonant Local Field Enhanced Visible Harmonic Generation in an Azo-Polymer Resonant Waveguide Grating. *Opt. Express* **2014**, *22* (3), 2790.
(46) Vu, D. T.; Chiu, H. W.; Nababan, R.; Le, Q. M.; Kuo, S. W.; Chau, L. K.; Ting, C. C.; Kan, H.-C.; Hsu, C. C. Enhancing Upconversion Luminescence Emission of Rare Earth Nanophosphors in Aqueous Solution with Thousands Fold Enhancement Factor by

Low Refractive Index Resonant Waveguide Grating. *ACS Photonics* **2018**, *5* (8), 3263−3271.
(47) Vu, D. T.; Tsai, Y. C.; Le, Q. M.; Kuo, S. W.; Lai, N. D.; Benisty, H.; Lin, J. Y.; Kan, H. C.; Hsu, C. C. A Synergy Approach to Enhance Upconversion Luminescence Emission of Rare Earth Nanophosphors with Million-Fold Enhancement Factor. *Crystals* **2021**, *11* (10), 1187.
(48) Barya, P.; Xiong, Y.; Shepherd, S.; Gupta, R.; Akin, L. D.; Tibbs, J.; Lee, H.; Singamaneni, S.; Cunningham, B. T. Photonic-Plasmonic Coupling Enhanced Fluorescence Enabling Digital-Resolution Ultrasensitive Protein Detection. *Small* **2023**, *19* (44), 2207239.
(49) Masson, J.; Battaglia, T.; Davidson, M.; Kim, Y.; Prakash, A.; Beaudoin, S.; Booksh, K. Biocompatible Polymers for Antibody Support on Gold Surfaces. *Talanta* **2005**, *67* (5), 918−925.
(50) Liberelle, B.; Merzouki, A.; Crescenzo, G. De. Immobilized Carboxymethylated Dextran Coatings for Enhanced ELISA. *J. Immunol. Methods* **2013**, *389* (1−2), 38−44.
(51) Liu, H. L.; Tseng, Y. T.; Lai, M. C.; Chau, L. K. Ultrasensitive and Rapid Detection of N-Terminal Pro-B-Type Natriuretic Peptide (NT-proBNP) Using Fiber Optic Nanogold-Linked Immunosorbent Assay. *Biosensors* **2022**, *12* (9), 746.
(52) Tzolos, E.; Adamson, P. D.; Hall, P. S.; Macpherson, I. R.; Oikonomidou, O.; MacLean, M.; Lewis, S. C.; McVicars, H.; Newby, D. E.; Mills, N. L.; Lang, N. N.; Henriksen, P. A. Dynamic Changes in High-Sensitivity Cardiac Troponin I in Response to Anthracycline-Based Chemotherapy. *Clin. Oncol.* **2020**, *32* (5), 292−297.

https://doi.org/10.1021/acssensors.3c02240
ACS Sens. 2024, 9, 455−463